JOURNAL OF MECHANICS OF CONTINUA AND MATHEMATICAL SCIENCES
www.journalimcms.org

ISSN (Online) : 2454 -7190 Vol.-19, No.-11, November (2024) pp 56 - 78 ISSN (Print) 0973-8975

DYNAMICS OF REINFORCED CONCRETE SLAB OF PEDESTRIAN BRIDGE WITH RIGID REINFORCEMENT

Anatoly Alekseytsev[1], Vincent Kvočak[2], Dmitry Popov[3], Mohamad Al Ali[4]

[1, 3] Department of Reinforced Concrete and Masonry Structures, Moscow State University of Civil Engineering, Russia

[2, 4] Department of Steel and Timber Structures, Technical University of Košice Russia.

Email: [1]aalexw@mail.ru, [2]vincent.kvocak@tuke.sk, [3]popovds89@mail.ru [4]mohamad.alali@tuke.sk

Corresponding Author: **Anatoly Alekseytsev**

https://doi.org/10.26782/jmcms.2024.11.00005

(Received: August 25, 2024; Revised: October 18, 2024; Accepted: November 02, 2024)

Abstract

The article is devoted to the actual problem of studying the dynamic response of bent plate structures with reinforcement represented by rigid metal profiles. Such structures can be used in pedestrian bridges or other span structures. A finite element model is built by using the example of a pedestrian bridge slab with reinforcement in the form of steel T-shape profiles. Deformations of concrete, reinforcement, and rigid reinforcement bars are described by a system of solid and shell finite elements, that take into consideration modern models of physical, geometric, and structural nonlinearity. The dynamic impact is modeled at low speed in two variants. The first is a blast load is applied in the middle of the span according to a symmetrical scheme, and the second pursuant to an asymmetric scheme. The structural and inertial damping of vibrations of the damaged system is taken into account. In this case, an implicit integration method is used. The time variation of the dynamic load implies a residual mass of the impacting body that vibrates with the slab structure after the onset of impact. The bond between concrete and stiff rebar is evaluated by the level of cohesion stresses in the vicinity of the profile with maximum strains. The finite element model is verified with a full-scale experiment in which a slab with rigid reinforcement is built and tested. Numerical studies have shown that asymmetrical loading can have a more negative effect on the structure than symmetrical loading, with structure deflections varying by up to 42%. As a result, the effectiveness of experimental theoretical modeling of the dynamics of such structures is shown, which can be used for both typical and individual designs.

Keywords: Dynamic load, Numerical simulation, Pedestrian bridge, Reinforced concrete.

I. Introduction

At the modern stage of designing the question of providing mechanical safety of building structures in conditions of various technogenic influences such as explosions, impulse shocks, effects of fire, etc. is becoming more and more necessary. Concrete, reinforced concrete, steel-fiber-reinforced concrete, and other composite structures are subjected to similar, often beyond-design effects [XXIII, XLI, XXXVIII, XIV, XV]. The solution to dynamics problems can be divided into low and high-speed load applications. Consideration of low-speed problems [III, VII], assumes a time-varying impulse load and numerical solution in an implicit formulation. In high-speed problems [VII, XX, XXVI, XLII], models with explicit solvers are often used. The failure criteria are von Mises stresses for steel and principal stresses for concrete, determined based on the Drucker-Prager plasticity model, Menetrey-Willam model, and others.

Bridge structures during their exploitation can experience various dynamic loads, such as train impacts [XXXIII], collisions with cars and ships [XXXIII, XL, XI, XII], rock impacts in mountainous areas [XXXIX, XXI]. Accordingly, pedestrian bridges can be subjected to similar dynamic impacts. The techniques of modeling such accident impacts belong to the elements of pull-down analysis [XXXVI, XXXV, XXXI, XXXIV, XXXVII, V] and methods of integration over implicit schemes [XVII, XXII, XIX].

Increasing the safety of structures experiencing such emergency loads is usually achieved by increasing the material capacity or reducing the oscillations of the system with the help of dampers. At the same time, the real effect can be achieved by local introduction of links or changes in stiffnesses leading to the necessary change of natural frequencies of vibrations of structures [III, XVIII]. This approach is implemented for the simplest beam systems with isotropic properties, whereas the solution to similar problems of complex structural systems is still possible only by means of numerical modeling.

One of the important and having several approaches to the solution is the problem of correct modeling of dynamic loads in software packages [IX, XXX, XXVIII, XXIX, XXV]. The first option modeling dynamic impact using impulse load, another approach is the combination of concentrated mass and gap, that is, there is a free fall of mass with the acceleration of gravity.

One of the important factors in obtaining a correct study of structures experiencing dynamic loading is damping. Damping can be numerical, which is necessary to stabilize the iterative process of solution and physical based on two Rayleigh variables α and β. The models of V.N. Sidorov [XXXII] and the Kelvin-Foigt model are also equally effective.

The paper performs numerical modeling of a symmetrically and asymmetrically dynamically loaded pedestrian bridge slab. Dynamic loading is modeled by a time-

varying impulse load, simulating the transfer of kinetic energy of an impacting body. The paper determines the limit static and dynamic loading of the slab, establishes the danger of asymmetric dynamic loading, and establishes the degree of influence of rigid reinforcement on the slab performance including after the limit load.

II. Methods and materials

II.i. Purpose of the study and problem statement

The purpose of the study is to evaluate the stress-strain state and ultimate load for bridge pedestrian floor slabs with rigid reinforcement under dynamic loading.

For this purpose, the following research program was developed:

- fabricate the pedestrian bridge slab and determine the limit static load experimentally;

- verify the finite element model with the results of experimental studies under static loading;

- build a numerical model of the pedestrian bridge slab under dynamic loading and analyze its stress-strain state under dynamic loading.

The subject of the study is a steel-reinforced concrete slab used for the slab of a pedestrian bridge. A metal profile is installed in the tension zone of this slab (see Fig. 1, a). The parameters of the slab are length - 6000 mm (distance between supports - 5800 mm); width - 900 mm; height - 270 mm.

The slab has flexible rebars and stirrups with a diameter of 12 mm and a rigid reinforcement. The rigid reinforcement is represented by two steel metal profiles of T-shaped form (turned by 90 degrees), each of them consisting of two parts: the bottom part made of solid sheet metal with a thickness of 9.2 mm (shelf) and ribs with a thickness of 5.9 mm. On the side surface of the profiles, there are holes with a diameter of 50 mm and a pitch of 100 mm.

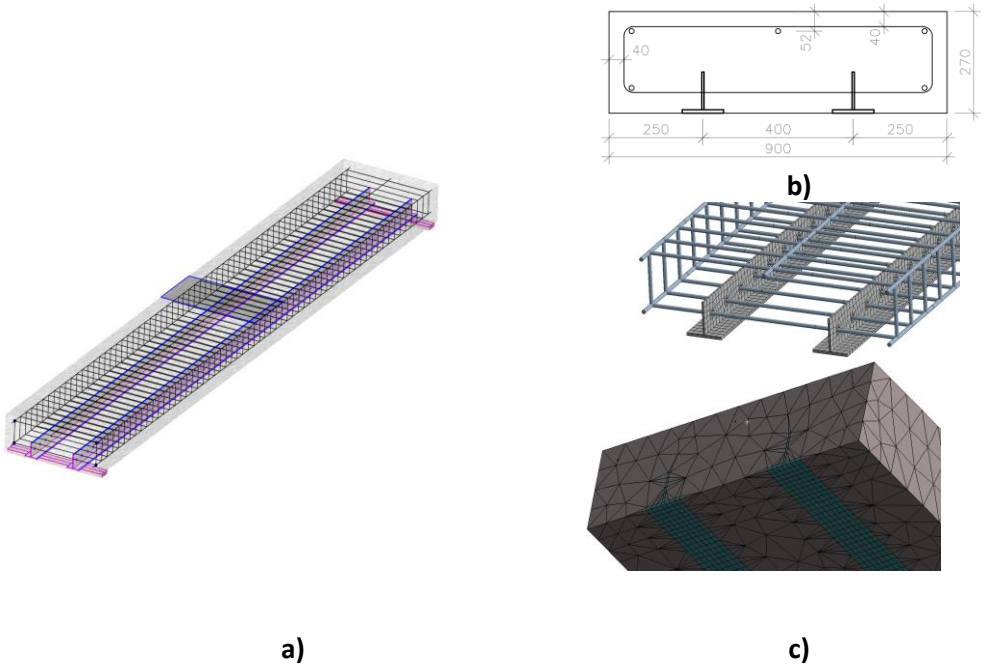

Fig 1. Object of study: (a) general view of the pedestrian slab; (b) normal section of the slab; (c) finite element model of the slab

II.ii. Numerical model of the structure

II.ii.a. Description of finite element model

Numerical modeling was performed in the Ansys software package. Partitioning of the slab model was performed in two stages in the first stage the rigid reinforcement was triangulated with the finite element size of 20mm, then the concrete part of the floor slab was partitioned with the element size of 75mm. This step-by-step approach and the size of the elements when creating the finite element mesh leads to the most accurate picture of the stress-strain state of the model and optimal calculation time. Calculation for static loads took one hour for dynamic loads of about five hours. Modeling of rigid reinforcement and concrete was performed using Solid 186 (20-node FE) and Solid 187 (10-node tetrahedral FE).

II.ii.b. Models of materials

The behavior of concrete is described using the Menetri-Willam model [VI], which is based on plastic flow theory. The Menetri-Willam model is generally more applicable to modeling the behavior of bound aggregates such as concrete than the Drucker-Prager model without modifications [XXVI].

1) The concrete model consists of three main components:

A triaxial failure surface f_{MW}, (Fig. 2,) is described by equation (1), where c_2 and c_3 are parameters of the equation that control the shape of the meridional cross-section of the surface and are determined from the yield strengths in uniaxial tension (R_t),

compression (R_c) and biaxial compression (R_b) [XXVII]. The limit surface expresses the strength state of the material in the Haig-Westergaard principal stress space. This surface contains a single point of singularity located at the apex, in the triaxial tensile region.

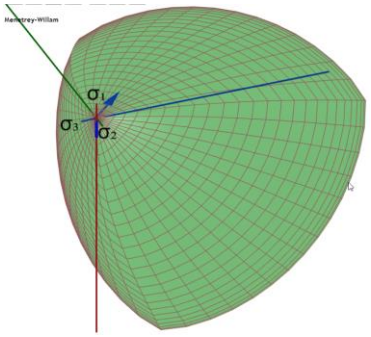

$$f_{MW} = \frac{c_2}{c_3}\left[\sqrt{2\xi} + rp\right] + p^2 - \frac{1}{c_3} \quad (1)$$

$$Q_{MW} = \rho^2 + B_g p + C_g \xi, \quad (2)$$

$$B_g = \frac{2 \cdot (\sqrt{2} \cdot tan(\Psi_b) \cdot R_b - R_{bt})}{\sqrt{3}\left(1/\sqrt{2} - tan(\Psi_b)\right)} \quad (3)$$

$$C_g = \frac{B_g}{\sqrt{2}} + 2 \cdot \frac{R_{bt}}{\sqrt{3}} \quad (4)$$

Fig 2. The limiting surface of the Menetrier-William model and basic expressions for its description

2) Plastic potential surface [X], responsible for the direction of the plastic strain vector, described by equations (2)-(4), where ψ_b is the dilatation angle of concrete in uniaxial compression, which is the result of dividing the norm of the volume plastic strain tensor by the norm of the plastic strain deviator; B_g and C_g parameters characterizing the plastic potential. The values of the dilatation angle depending on the concrete mixture class are based on the assumption that when the strength surface is reached in uniaxial compression, the total volumetric strains are equal to zero [VIII]:

$$\Psi_b = \frac{R_b(1-2v)\cdot\sqrt{2}}{|2\cdot R_b(v+1)-3\cdot\varepsilon_0\cdot E_b|}, \; pa\partial;$$
$$\varepsilon_0 = \frac{(18+R_b)\cdot(62\cdot R_b + 0.675\cdot R_b^2 + 22)}{(53000-62\cdot R_b)\cdot(7\cdot R_b + R_b^2 + 22)} \quad (1)$$

where υ, E_b are Poisson's ratio and elastic modulus, respectively; ε_0 is the absolute value of axial relative strains that correspond to the uniaxial compression strength limit R_b.

3) Strengthening and de-strengthening of the material is determined by the laws of evolution of the ultimate surface. The work of concrete in compression (Fig. 3, a) and tension (Fig. 3, b) is not treated in the same way and is described by an exponential law (Exponential softening in compression and tension).

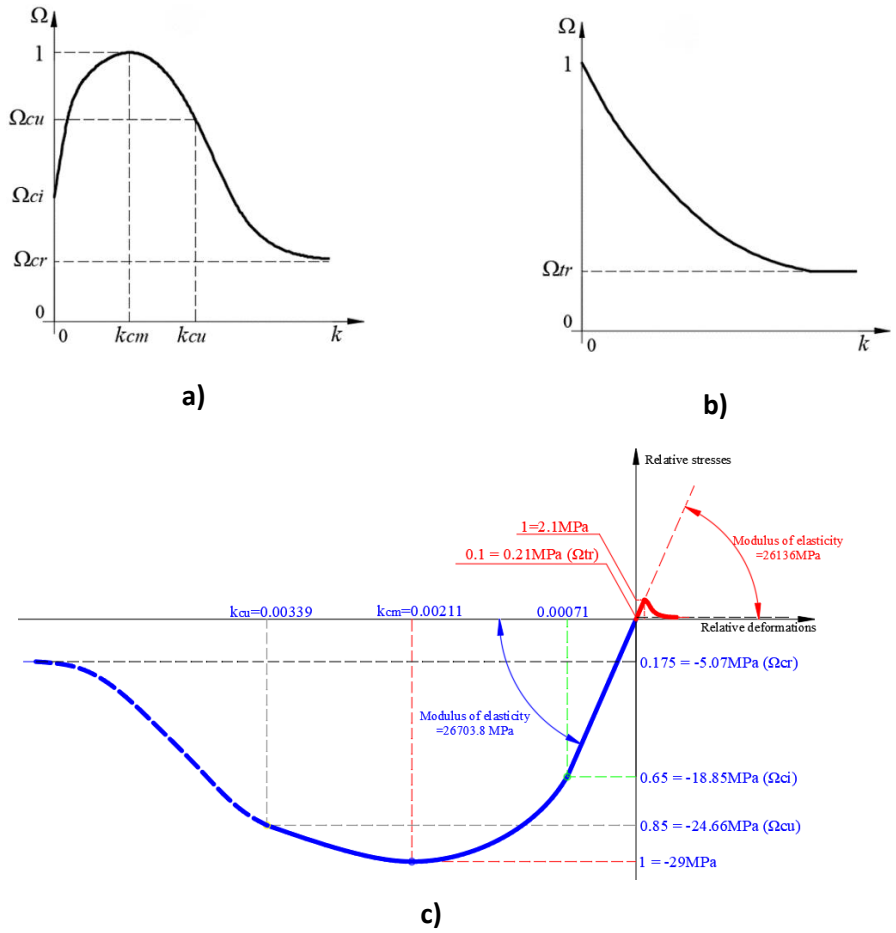

Fig. 3. The laws of hardening (a) and softening (b) of concrete, as well as a diagram of concrete deformation with strength values (c)

The exponential law is defined by normal stresses and plastic deformations given following the recommendations of SP 63.13330.2018. The specific points on the concrete performance diagram are found as the difference between the total deformations at relative stress Ω=1.0 and Ω =0.85 and the elastic deformations obtained at relative stress level Ω =0.65. Figure 3, c shows the concrete diagram considered in the calculation of the bridge pedestrian slab.

One of the parameters that characterize the material failure in tension is the fracture energy G_F [XXIV]. This parameter represents the amount of energy that must be imparted to the material to stop the transfer of stresses between the edge of the crack propagation (to completely break the interatomic bonds). Graphically, this value represents the area under the plot of stress versus crack opening width (Fig. 4). The deformation of rigid reinforcement was described by a multilinear relationship with hardening (Fig. 5), the values of strains in the diagrams of steelwork, as well as concrete are taken in Ansys plastic, elastic work is determined based on the value of the modulus of elasticity.

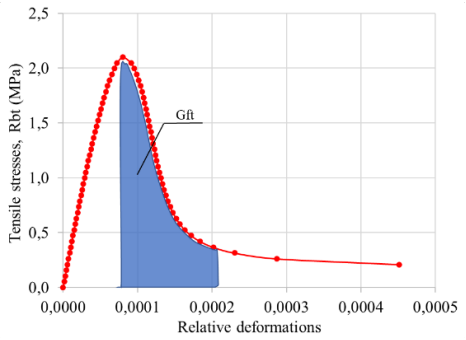

Fig. 4. Fracture energy G_F on the tensile diagram of concrete

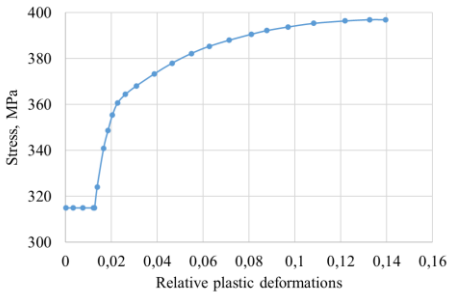

Fig. 5. Multiple linear diagrams of rigid reinforcement deformation

The strength characteristics of concrete and steel used in the numerical calculation were determined based on experimental studies [I]. Structural reinforcement of the slab with individual (flexible) bars was performed by discrete finite elements REINF264, which allows not to perform the partitioning of the finite element mesh in such a way that the bar elements are connected to the nodes of the volume elements (modeling concrete), hence a better mesh for the models can be obtained [IIXIII]. The behavior of ordinary reinforcing steel is described by a bilinear relationship with a yield strength of 400 MPa.

II.ii.c. Support anchorages and slab loading

The support parts of the slab are modeled by metal flat bars, with the bar itself connected to the slab without contact and split into two parts. The separation line of one support is hinged (Fig. 6b) and the second support is hinged and fixed. Studies have shown that this method of modeling boundary conditions more accurately reflects the real work of the support connections with the slab, does not create additional forces in the bearing zone and allows for rotation, preventing the occurrence of the supporting bending moment.

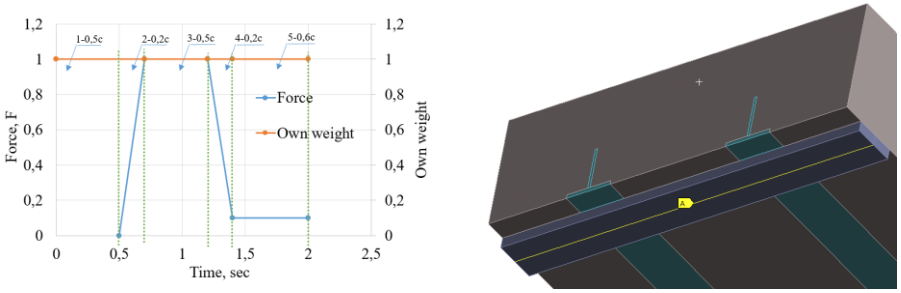

a) b)

Fig. 6. Time variation of loads (a) boundary conditions (b)

The bridge slab model was calculated by applying the load in two different zones (Fig. 7), which corresponds to the most dangerous load positions. The load in time was applied to the slab in four stages (Fig. 6a).

The first stage was the application of own weight in 0.5 sec; the second stage was the increase of dynamic load in 0.2 sec; the third stage was the stabilization of load at the maximum value in 0.5 sec; the fourth stage was the reduction of dynamic load to 10% of the peak value in 0.2 sec.

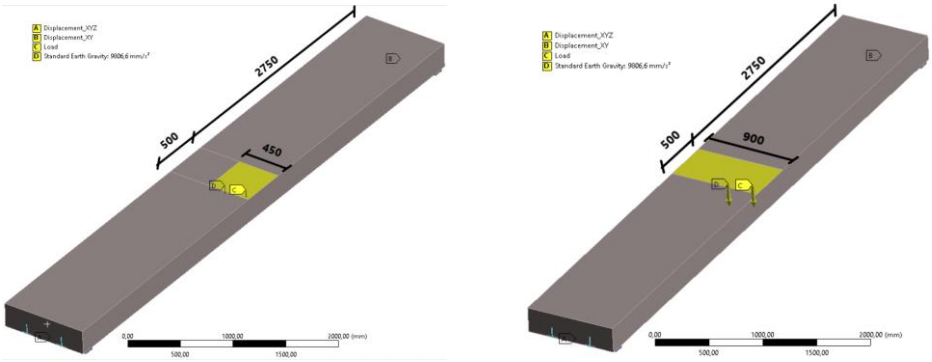

a) b)

Fig. 7. Unsymmetrical (a) and symmetrical (b) location of the loading area of the slab

The basic concept of dynamic load application (Fig. 6, a) is as follows:

- applying its own weight and stabilizing the vibrations (first stage),

- growth of impulse load, which simulates, for example, the fall of bodies on the bridge with acceleration, free fall, or other man-made impact (second stage),

- the maximum effect of the impulse for some time (third stage),

- drop of the impulse load and vibrations of the structure together with the impacting body (fourth stage).

The maximum value of impulse loading was defined as 80% under static loading capacity (determined at the first stage of calculation). In the case of the application of a load of more than 80%, plastic deformations are achieved in reinforcement and concrete in significant areas, which leads to destabilization of natural vibrations and loss of the whole picture of the structure under load. The reason for this effect is the inertial component of dynamic effects, which at the beginning of the third stage of loading (Fig. 14) leads to exceeding the capacity of static load.

II.ii.d. Description of the finite element solver.

The Static Structural module of Ansys was used to determine the static load capacity of the slab. Further, the Modal analysis module was used to determine the natural

frequencies of vibration required for the physical damping. The solution of dynamics problems taking into account inertial and damping forces in Ansys allows to performance of the Transient Structural module based on implicit schemes of integration of the equation of motion. One of the important properties of the Transient Structural module is that it can be used in conjunction with the Static Structural model. In this case, all the parameters of materials (concrete, reinforcement, concrete hardening, etc.), boundary conditions, and loads can be used without modification in the calculation, except for the setting of the dynamic calculation parameters.

The equation of motion used to analyze the dynamic response of structures [VI]:

$$F(t) = [M]\{\ddot{u}\} + [C]\{\dot{u}\} + [K]\{u\}, \quad (6)$$

where, [M] is the mass matrix, [C] is the damping matrix; [K] is the stiffness matrix; F(t) is the load; $\{\ddot{u}\}$ it is the node acceleration vector; $\{\dot{u}\}$ it is the node velocity vector; $\{u\}$it is the node displacement vector. At any point in time, these equations can be represented as a set of "static" equilibrium equations that also take into account inertia forces $[M]\{\ddot{u}\}$) and damping forces ($[C]\{\dot{u}\}$). The Transient Structural module applies the Newmark time integration method to solve the equations at specific points in time. Damping is an important parameter in dynamic loading. Two types of damping can be configured in Ansys: numerical and physical. Numerical (artificial) damping is used to stabilize the solution. There are several types of Newmark parameter solver settings α and δ that use the same system of equations:

$$\delta = \frac{1}{2} + \gamma\,; \quad \alpha = \frac{1}{4}(1+\gamma)^2, \quad (7)$$

where, γ is the value of numerical damping.

The value of numerical damping is constant depending on the selected type of solver setup, that is: Impact - γ =0; High-speed dynamics - γ =0.005; Moderate speed dynamics - γ =0.1; Low-speed dynamics - γ = 0.414;

The physical damping was accounted for using Rayleigh constants α and β. The damping matrix [C] is calculated using these constants multiplied by the mass matrix [M] and the stiffness matrix [K]:

$$[C] = \alpha[M] + \beta[K] \quad (8)$$

There are two ways to consider physical damping in Ansys: "Direct input" and "Damping vs Frequency". In the first method ("Direct input"), the Rayleigh alpha and beta coefficients are given specific numerical values. For this calculation, the second method, "Damping vs Frequency" is chosen, where the following parameters are used:

- frequency of natural oscillations (ω), determined in the module "Modal analysis" and amounted to 13.7Hz;

- damping coefficient (ξ), for reinforced concrete it is equal to 0.05;

- the alpha coefficient is taken to be zero since the external environment has no influence;

- the value of the beta coefficient is determined automatically in the solver.

II.iii. Experimental verification of the numerical model of the structure

To verify the results obtained with the numerical model, calculations were carried out with conditions and characteristics that correspond to the experimental tests, bridge slab with rigid reinforcement bent into U - shape [I].

The calculation model used the material characteristics obtained during the tests: cylindrical strength of concrete - 32.17 MPa; yield strength and steel tensile strength of rigid reinforcement - 315 MPa and 396 MPa, respectively; yield strength of flexible reinforcement - 355 MPa. Figure 8 shows the graphical dependence of the slab deflection on the load for the experimental specimen and the numerical model.

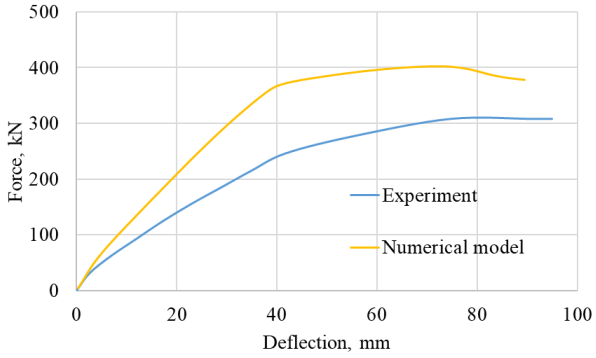

Fig. 8. Dependence of deflection on load in experimental and numerical models

The comparative analysis of the load-deflection dependences in the experimental specimens with the results of numerical calculation showed good correspondence. The difference between the numerical and experimental values of deflections is about 3%, and the difference in failure forces does not exceed 24%. This indicates the correctness of modeling of strength and stiffness characteristics of materials, types of finite elements, boundary conditions, as well as models of concrete and reinforcement behavior. As a result of conformity with experimental studies, it allows to perform numerical calculations of similar slabs.

The general view of experimental specimens and experimentation is presented in Figure 9.

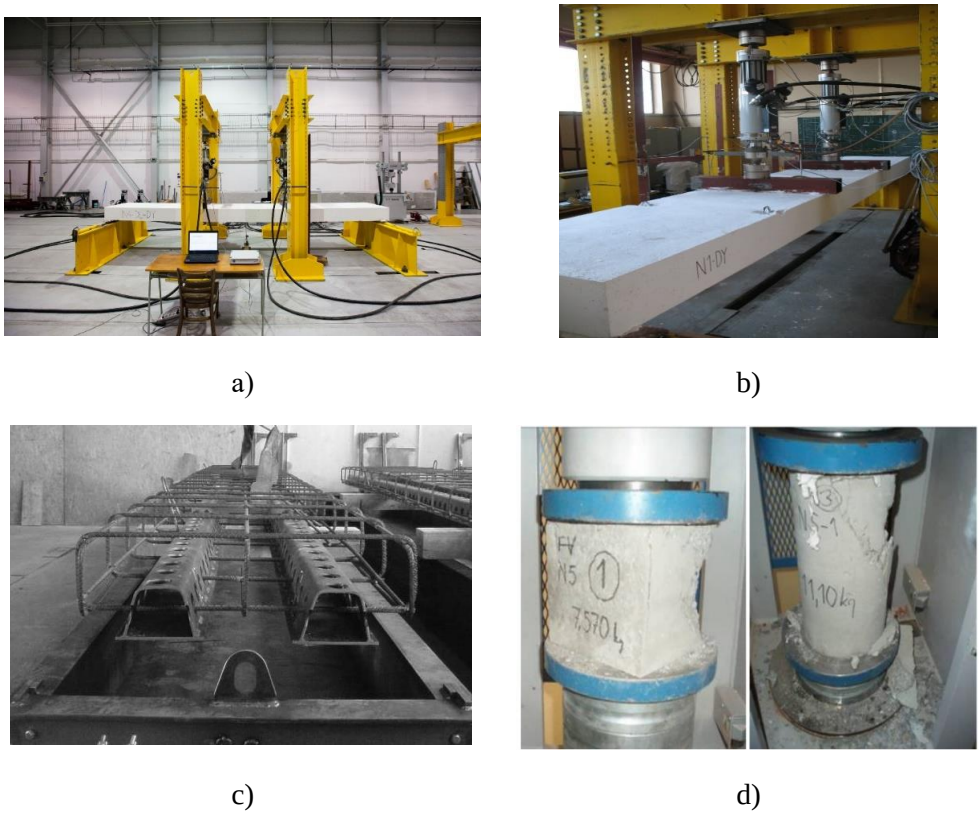

a) b)

c) d)

Fig. 9. Experimental tests of a pedestrian bridge slab: general view of the stand (a) load application scheme (b), reinforcement frame (c), testing of concrete specimens for cubic and cylindrical strength (d)

The compressive strength of the concrete specimens (Fig. 9,d) and the tensile strength of the reinforcement were experimentally determined beforehand. Then the pedestrian slab specimens were produced, the reinforcement scheme of which is shown in Fig. 9,c. The slab specimens were mounted on a steel frame (Fig., a) and brought to static loading capacity using two force plates (Fig. 9, b). Experimentally determined mechanical characteristics of the materials and average values of the geometry measured on the specimen were used in the calculations.

III. Results

Numerical calculations of the models in static and dynamic staging resulted in the determination of the ultimate load and deflection values under symmetric and asymmetric loading.

The maximum static load and deflection under unsymmetrical loading are 192.01 kN and 59.57 mm, and under dynamic loading are 205.8 kN and 61.6 mm, respectively. In the case of symmetrical loading, the ultimate static load is 188.5 kN and the deflection is 49.5 mm. In the case of dynamic loading, these values are 204.9 kN and 41.1 mm, respectively (Fig. 10).

The ultimate bearing capacity values under static and dynamic loading of symmetrically and asymmetrically loaded slabs differ by no more than 8%. The ultimate deflection of the asymmetrically loaded slab under static loading is higher by 20% under dynamic loading by 49%. These results show that asymmetrical accidental impacts pose a great danger for such structures.

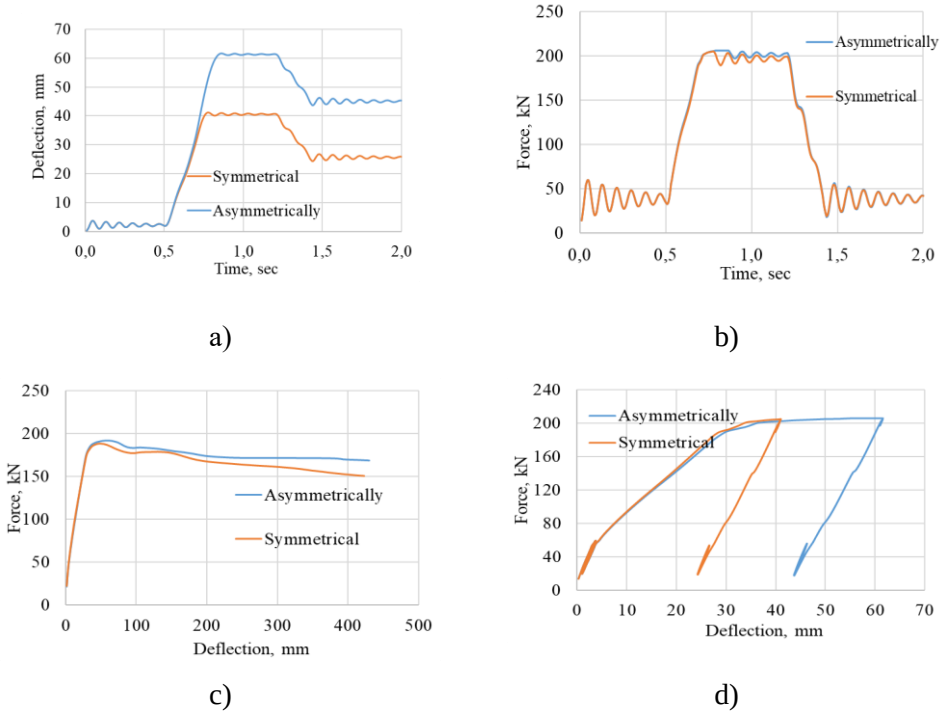

Fig. 10. Time variation of deflection (a) and load (b), N-f dependence under static (c) and dynamic (d) loading

Figure 11 shows the normal cross sections in the middle of the pavement slabs, which show the normal stresses in concrete and reinforcement under the maximum dynamic load. It is possible to notice the difference in values of arising forces, so in the compressed zone of concrete under asymmetric loading, the maximum forces are 29,0MPa, which is more than the exact prism strength, and such values can be characterized as the beginning of the failure of the compressed zone of the slab. At the same time, the values of compressive stresses in the concrete of the slab loaded symmetrically are 26.0MPa and do not exceed the cylindrical strength.

In the meantime, for symmetrical loading, the lower part of both bars of the rigid working reinforcement undergoes significant plastic deformations and is in the hardening zone with a bearing capacity reserve of 23% (at a time resistance of 390 MPa). In the case of asymmetric loading, the left bar of the rigid reinforcement works elastically, while the right one has a 21% safety margin in terms of time resistance. All this confirms that dynamic asymmetric loading is the most dangerous in terms of the

limited state of the structure. In addition to normal stresses used for preliminary assessment of the stress state of concrete and reinforcement, Mises equivalent stresses in rigid reinforcement and principal stresses, in concrete were calculated. Qualitatively, the stress state of the slab elements is the same as in the normal stress analysis only.

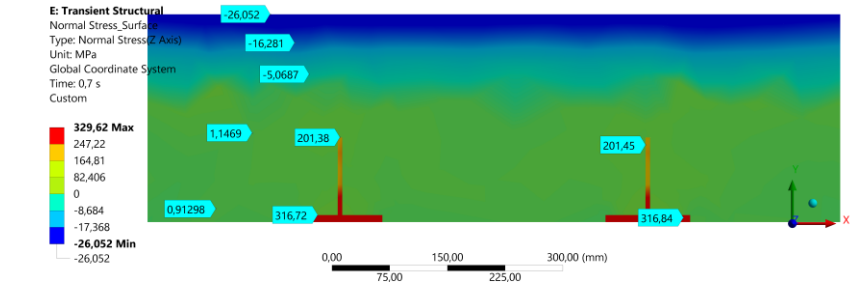

a)

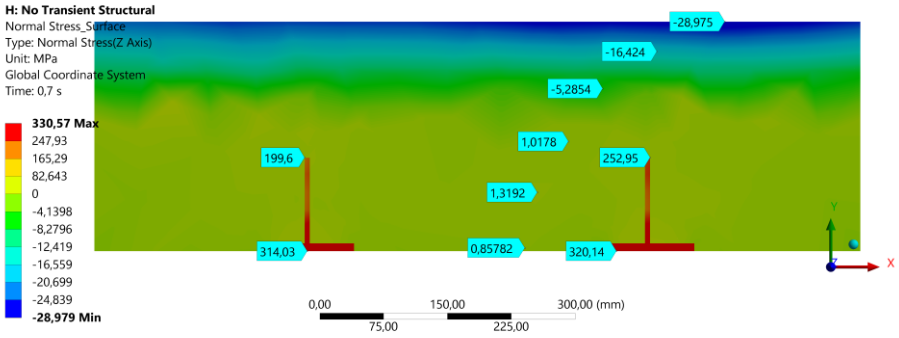

b)

Fig. 11. Stresses in the slab section under symmetrical (a) and asymmetrical loading (b)

When analyzing the variation of normal stresses in time according to Fig. 6, characteristic states were considered:

- normal operation loading (t=0.5 c);

- growth of dynamic loading up to the peak value (t=0.7 c);

- action of maximum dynamic loading (t=1.2 c);

- the moment of unloading - the beginning of vibrations together with the striking body (t=1.4 c)

The distribution of stresses in the structure corresponding to these moments of time is shown in Fig.12. The analysis of the figure shows that the stresses in concrete at the moment of the beginning and the end of the peak dynamic load do not stabilize, but increase.

Symmetrical load

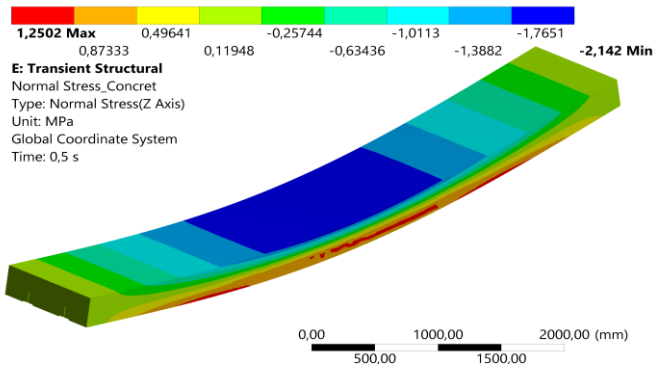

t=0.5 c

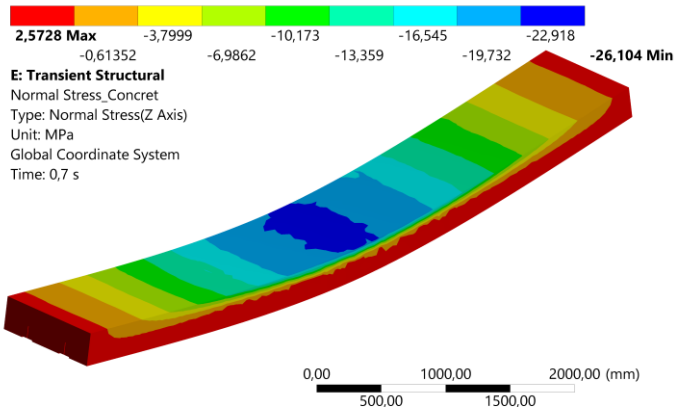

t=0.7 c

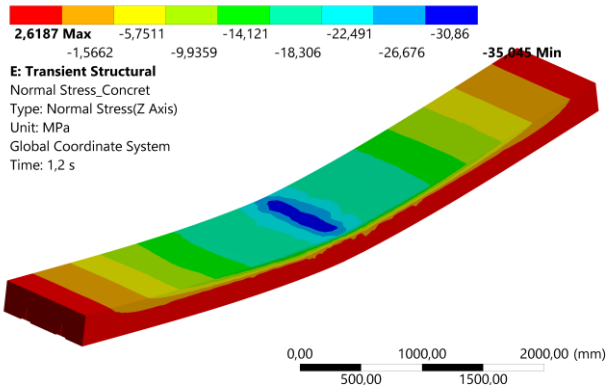

t=1.2 c

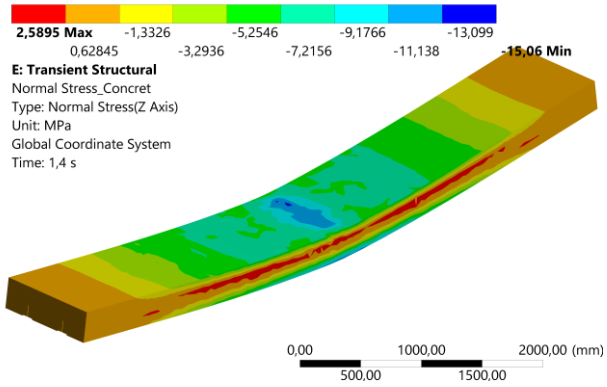

t=1.4 c

Unsymmetrical load

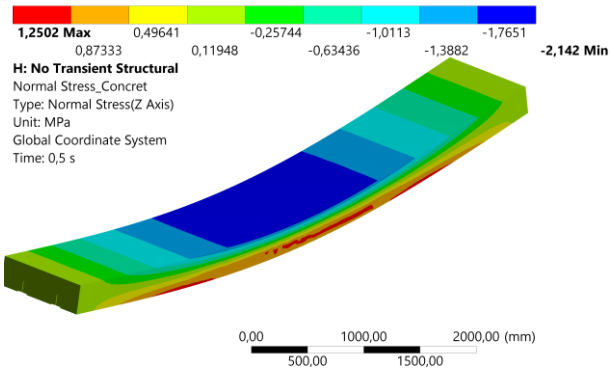

t=0.5 c

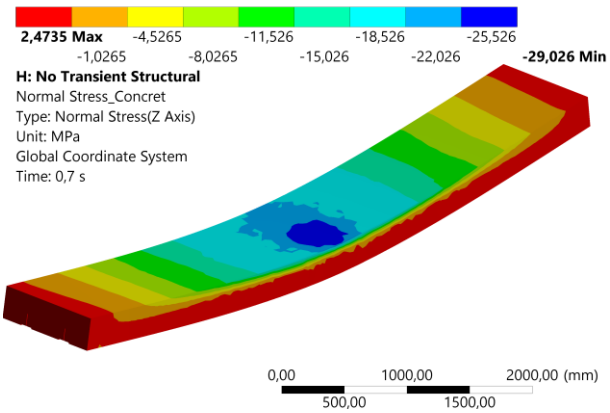

t=0.7 c

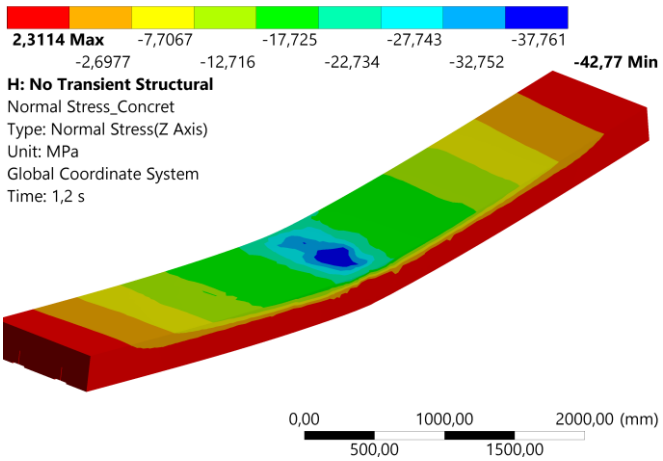

t=1.2 c

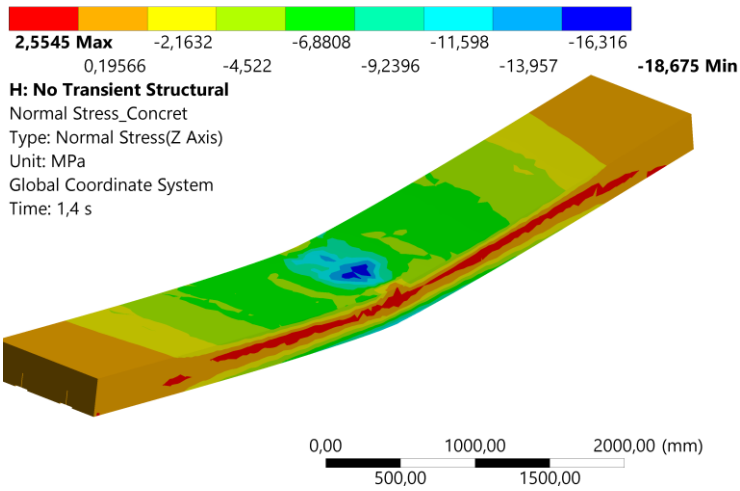

t=1.4 c

Fig. 12. Time variation of stresses in slab concrete

This indicates the importance of taking into account the time of application of peak dynamic load, which, if applied for a longer time than 1.2-0.7= 0.5 s, may lead to the complete collapse of the structure. In addition, at the moment of unloading, tensile stresses significant for crack formation occur in the middle part of the slab. In the lower zone, the slab is compressed. In further analysis of joint vibrations, the concrete tensile zone extends to the upper part of the slab in the vicinity of the dynamic load application. All this allows us to conclude that the failure of this construction predominantly occurs in concrete.

Figure 13 shows a plot of the variation of the bearing capacity of a symmetrically loaded slab, where it can be observed that the slab is quite prolonged after reaching the maximum value of the external load.

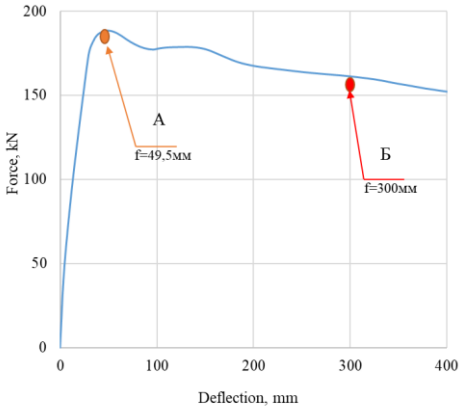

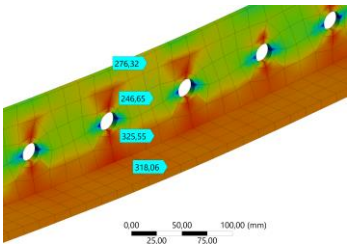

a) Point A

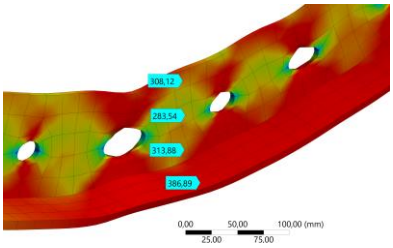

b) Point B

Fig. 13. N-f dependence of the numerical model of the slab. Point A - stresses in the rigid reinforcement at maximum external load. Point B - stresses in rigid reinforcement at significant deflection of the slab.

Applying an initial dynamic load of more than 80% of the static load leads to significant deformations of concrete and reinforcement, and the values of the specified dynamic load are not achieved, Figure 14 shows the graph of load versus time when comparing it with the graph in Figure 10b, the destabilization of natural vibrations and the loss of a complete picture of the structure under load can be clearly seen.

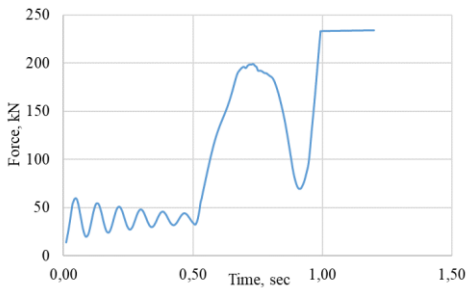

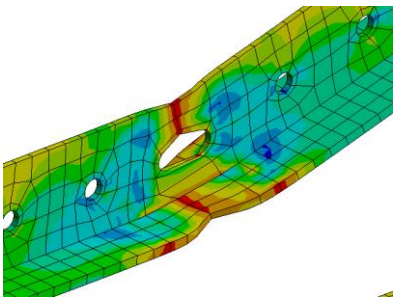

Fig. 14. Time variation of load (a) and deformation of rigid reinforcement (b).

Consequently, the danger of dynamic or beyond-design loads caused by accidental anthropogenic impacts leads to the necessity of studying such cases of structural operation.

IV. Discussion

To evaluate the performance of floor slabs with rigid reinforcement after reaching the load capacity, additional calculations were performed. It was determined that even after reaching the limit values of the criterion of survivability in deflection, equal to 1/30 of the span, that is, 20 cm (600 / 30 = 20), did not lead to the destruction of the structure, even when reaching a deflection of 30 centimeters, the bearing capacity of the slab was preserved. Preservation of the bearing capacity and integrity of the structure after reaching the ultimate load is due to the work of the rigid reinforcement. After the loss of adhesion with concrete in the lower zone, the rigid reinforcement of the slab begins to work on the principle of a beam, and then as a cable-stayed mechanism, the load-bearing capacity of the slab is determined by the load-bearing capacity of the profile of rigid reinforcement. As a result of this study, it can be said that the use of rigid reinforcement in bending reinforced concrete elements practically excludes the possibility of complete emergency collapse of structures, which indicates an increase in their survivability. Thus, the use of rigid reinforcement in bending reinforced concrete elements increases the survivability of the structure and ensures its safety in case of various impacts. Additional studies will allow us to specify the survivability criteria for such structures and optimize their design. In general, rigid reinforcement is one of the effective ways to increase the reliability and strength of reinforced concrete structures.

The initial value of dynamic load when searching for its limiting value was taken as 85% (asymmetrical loading - 162.8kN, symmetrical loading - 158.5kN) of the static value, but according to the calculation results, the maximum value exceeded the static value by 26.4% (205.8kN) under asymmetrical loading and by 29.2% (204.9kN) under symmetrical loading, which may be due to the occurrence of inertial effects and strengthening of materials. It is also worth noting that if in the calculation of the model with asymmetrical loading (in which the dynamic load of 162.8kN is applied), the limiting value of the load of the symmetrical model (158.5kN) is used, then the values of the obtained limiting dynamic load and deflection will be 204, 8kN and 43.33cm, respectively, i.e. the ultimate load remains approximately at the same level, while the deflection decreases by 42% (1-61.6/43.3=42%) Proving again that it is the asymmetric accidental impacts that pose the greatest danger to such structures.

V. Conclusion

1. A methodology for modeling the deformations of pedestrian slabs under blast load has been developed, which provides for the use of experimentally verified volumetric finite element schemes that reproduce the real dynamic response of the structure.

2. It is established that the rigid reinforcement of the considered profile increases the safety of the slab in comparison with the reinforcement with flexible reinforcement, while the asymmetric impact is the most unfavorable about the symmetric one, in particular:

- according to the calculation results, the maximum value exceeded the static value by 26.4% (205.8kN) under asymmetric loading and by 29.2% (204.9kN) under symmetric loading, which may be due to the occurrence of inertial effects and material hardening.

- When calculating the model with asymmetrical loading (in which dynamic load of 162.8 kN is applied), to use the limiting value of loading of the symmetrical model (158.5 kN), then the values of the obtained limiting dynamic load and deflection will be 204.8 kN and 43.33 cm, respectively, that is, the limiting force remains approximately at the same level, and the deflection decreases by 42% (1-61.6/43.3=42%). This proves that it is the asymmetric failure impacts that pose a great danger to such structures.

3. The results of the calculation of the structure with different profiles of rigid reinforcement showed significantly different resistance of the structure to accidental impacts, which indicates the need to find rational solutions for the parameters of rigid reinforcement.

Conflicts of interest

All authors declare that they have no conflicts of interest.

References

I. Al Ali, Mohamad & Kvočák, Vincent & Dubecký, Daniel & Alekseytsev, Anatoliy. (2023). Experimental research on composite deck bridges with encased steel beams. Delta University Scientific Journal. 6. 31-38. 10.21608/dusj.2023.291004.

II. Alekhin V, Budarin A, Pletnev M, Avdonina L. MATEC Web of Conferences. 2019. 279 (02):02005. DOI: 10.1051/matecconf/201927902005

III. Alekseytsev A., Gaile L., Drukis P., : "Optimization of Steel Beam Structures for Frame Buildings Subject to Their Safety Requirements." *DOAJ (DOAJ: Directory of Open Access Journals)*, Nov. 2019, 10.18720/mce.91.1.

IV. Alekseytsev A., Sazonova S. : Numerical Analysis of the Buried Fiber Concrete Slabs Dynamics under Blast Loads. *Magazine of Civil Engineering* 2023, 117, doi:10.34910/MCE.117.3.

V. Alekseytsev, A., : "Mechanical Safety of Reinforced Concrete Frames Under Complex Emergency Actions." *DOAJ (DOAJ: Directory of Open Access Journals)*, Apr. 2021, https://doi.org/10.34910/mce.103.6.

VI. Ansys 2021. Mechanical APDL feature archive.

VII. Bregoli Guido, et al. "Static and Dynamic Tests on Steel Joints Equipped With Novel Structural Details for Progressive Collapse Mitigation." *Engineering Structures*, vol. 232, Jan. 2021, p. 111829. https://doi.org/10.1016/j.engstruct.2020.111829.

VIII. Budarin A.M., Rempel G.I., Kamzolkin A.A., Alekhin V.N. Concrete damage–plasticity model with double independent hardening. Vestnik MGSU [Monthly Journal on Construction and Architecture]. 2024;19(4):527-543. (In Russ.) https://doi.org/10.22227/1997-0935.2024.4.527-543

IX. Chen Y., May I., : "Reinforced Concrete Members Under Drop-weight Impacts." *Proceedings of the Institution of Civil Engineers - Structures and Buildings*, vol. 162, no. 1, Jan. 2009, pp. 45–56. https://doi.org/10.1680/stbu.2009.162.1.45.

X. Dmitriev A., Novozhilov Y., Mikhalyuk D., Lalin, V. Calibration and Validation of the Menetrey-Willam Constitutive Model for Concrete // Construction of Unique Buildings and Structures. 2020. Volume 88. Article No 8804. pp. 84-91.

XI. Fan Wei, et al., : "Reinforced Concrete Bridge Structures Under Barge Impacts: FE Modeling, Dynamic Behaviors, and UHPFRC-based Strengthening." *Ocean Engineering*, vol. 216, Sept. 2020, p. 108116. 10.1016/j.oceaneng.2020.108116.

XII. Fu Tao, et al., : "Study on the Time-dependent Reliability of Corroded Reinforced Concrete Bridge Structures Due to Ship Impact." *Advances in Civil Engineering*, vol. 2022, Jan. 2022, pp. 1–13. 10.1155/2022/8190297.

XIII. Inelastic analysis of structures, Milan J, Zdeněk P. ISBN 0-471-98716-6, 758 Pages. 10.1007/s00158-002-0217-z

XIV. Isaac, O.S.; Jagadeesh, G. Impulse Loading of Plates Using a Diverging Shock Tube. *Exp Mech* **2020**, 60, doi:10.1007/s11340-019-00573-5.

XV. Kasilingam S., Sharma R., Senthil R., Iqbal M., Gupta N., : "Influence of Reinforcement Bar on the Performance of Reinforced Concrete Slab Under Impact Loading." Springer Proceedings in Materials, 2023, pp. 331–42. 10.1007/978-981-99-6030-9_29.

XVI. Korsun V.I., Karpenko S.N., Makarenko S.Yu., Nedoresov A.V. Modern strength criteria for concrete under triaxial stress states. Building and Reconstruction. 2021;(5):16-30. 10.33979/2073-7416-2021-97-5-16-30

XVII. Kristoffersen, M., Hauge K., Minoretti A., Børvik T., : "Experimental and Numerical Studies of Tubular Concrete Structures Subjected to Blast Loading." Engineering Structures, vol. 233, Feb. 2021, p. 111543. 10.1016/j.engstruct.2020.111543.

XVIII. Kumpyak, O., Galyautdinov Z., Kokorin D., : "Strength of Concrete Structures Under Dynamic Loading." *AIP Conference Proceedings*, Jan. 2016, https://doi.org/10.1063/1.4937876.

XIX. Li Z., Zhang X., Shi Y., Wu C., Li J., : "Finite Element Modeling of FRP Retrofitted RC Column Against Blast Loading." *Composite Structures*, vol. 263, Feb. 2021, p. 113727. https://doi.org/10.1016/j.compstruct.2021.113727.

XX. Li Zhong-Xian, et al. "Finite Element Modeling of FRP Retrofitted RC Column Against Blast Loading." *Composite Structures*, vol. 263, Feb. 2021, p. 113727. 10.1016/j.compstruct.2021.113727.

XXI. Liu Z., Lu Z., Li Y., Hu R, Tu B., : "Study on Impact Resistance of Flexible Shed Tunnel for Bridges in Mountainous Areas". *Tiedao Xuebao/Journal of the China Railway Society* 2023, 45. doi:10.3969/j.issn.1001-8360.2023.03.015.

XXII. Maazoun A., Matthys S., Belkassem B., Atoui O., Lecompte, D., : "Experimental Study of the Bond Interaction Between CFRP and Concrete Under Blast Loading." *Composite Structures*, vol. 277, Aug. 2021, p. 114608. 10.1016/j.compstruct.2021.114608.

XXIII. Mahmoud Khaled Ahmed. : "Lateral Deformation Behavior of Eccentrically Loaded Slender RC Columns With Different Levels of Rotational End Restraint at Elevated Temperatures." *Journal of Structural Fire Engineering*, vol. 12, no. 1, Sept. 2020, pp. 35–64. 10.1108/jsfe-04-2020-0014.

XXIV. Menetrey P. Numerical analysis of punching failure in reinforced concrete structures, PhD thesis, Ecole Polytechnique Federale de Lausanne, Lausanne. 1994. p. 179.

XXV. Minhas A., None S., : "Numerical Simulation of Projectile Impact on Reinforced Concrete Structures: A Study of Slab Performance Under Varying Projectile Velocities Using ANSYS." Innovative Infrastructure Solutions, vol. 9, no. 10, Sept. 2024, 10.1007/s41062-024-01671-7.

XXVI. Mishra N, Netula, O., : "Behaviour of Reinforced Concrete Framed Structure Subjected to Blast Loading". *International Journal of Advanced Research in Engineering and Technology (IJARET)* 2021, 12, pp: 173-181. 10.34218/ijaret.12.1.2021.014

XXVII. Model Code for Concrete Structures 2010. International Federation for Structural Concrete, 2013. ISBN: 978-3-433-03061-5, 434 p

XXVIII. Ngo T., Mendis P., : Ngo, Tuan, and Priyan Mendis. "Modelling the Dynamic Response and Failure Modes of Reinforced Concrete Structures Subjected to Blast and Impact Loading." *STRUCTURAL ENGINEERING AND MECHANICS*, vol. 32, no. 2, May 2009, pp. 269–82. 10.12989/sem.2009.32.2.269.

XXIX. Niroomandi A., Pampanin S., Dhakal R., Ashtiani M., De La Torre C., : "Rectangular RC walls under bi-directional loading: recent experimental and numerical findings". *The Concrete NZ Conference,* 2018.

XXX. Qasrawi Y., Heffernan P., Fam A., : Qasrawi, Yazan, et al. "Dynamic Behaviour of Concrete Filled FRP Tubes Subjected to Impact Loading." *Engineering Structures*, vol. 100, June 2015, pp. 212–25. 10.1016/j.engstruct.2015.06.012.

XXXI. Shokrabadi M., Henry B., : "Risk-based Assessment of Aftershock and Mainshock-aftershock Seismic Performance of Reinforced Concrete Frames." *Structural Safety*, vol. 73, Mar. 2018, pp. 64–74. 10.1016/j.strusafe.2018.03.003.

XXXII. Sidorov V., Badina E., Detina E. Sidorov V., : "Nonlocal in time model of material damping in composite structural elements dynamic analysis." *International Journal for Computational Civil and Structural Engineering*, vol. 17, no. 4, Dec. 2021, pp. 14–21. 10.22337/2587-9618-2021-17-4-14-21.

XXXIII. Siguerdjidjene H., Leonid D., : "Study of Dynamic Impact of Speed Trains on Bridge Structures." *International Journal of Mechanics*, vol. 15, Mar. 2021, pp. 30–36. 10.46300/9104.2021.15.4.

XXXIV. Sinković L., et al., : "Risk-based Seismic Design for Collapse Safety." *Earthquake Engineering & Structural Dynamics*, vol. 45, no. 9, Mar. 2016, pp. 1451–71. 10.1002/eqe.2717.

XXXV. Sinković L., Matjaž D., : "Fatality Risk and Its Application to the Seismic Performance Assessment of a Building." *Engineering Structures*, vol. 205, Dec. 2019, p. 110108. https://doi.org/10.1016/j.engstruct.2019.110108.

XXXVI. Terrenzi, M., et al. "Collapse Limit State Definition for Seismic Assessment of Code-conforming RC Buildings." *International Journal of Advanced Structural Engineering*, vol. 10, no. 3, Sept. 2018, pp. 325–37. 10.1007/s40091-018-0200-6.

XXXVII. Thai, D.K., Pham, T.H., Nguyen, D.L. Thai, Duc-Kien, et al. "Damage Assessment of Reinforced Concrete Columns Retrofitted by Steel Jacket Under Blast Loading." *The Structural Design of Tall and Special Buildings*, vol. 29, no. 1, Nov. 2019, 10.1002/tal.1676.

XXXVIII. Yilmaz Tolga, et al. : "Experimental Investigation of Axially Loaded Reinforced Concrete Square Column Subjected to Lateral Low-velocity Impact Loading." *Structural Concrete*, vol. 20, no. 4, Apr. 2019, pp. 1358–78. 10.1002/suco.201800276.

XXXIX. Zhang Jingfeng, et al., : "A Comprehensive Approach for Bridge Performance Evaluation Under Rockfall Impact Integrated With Geological Hazard Analysis." *Engineering Failure Analysis*, vol. 141, Aug. 2022, p. 106668. 10.1016/j.engfailanal.2022.106668.

XL. Zhao Wuchao, et al., : "Performance of Bridge Structures Under Heavy Goods Vehicle Impact." *Computers and Concrete, an International Journal*, vol. 22, no. 6, Dec. 2018, p. 515. 10.12989/cac.2018.22.6.515.

XLI. Zheng X., Song J., Liu L., Sun B., Gao Z., : "Static and Dynamic Load Test on Concrete Hollow-core Slab Bridge." *Advances in Engineering Technology Research*, vol. 11, no. 1, July 2024, p. 327. 10.56028/aetr.11.1.327.2024.

XLII. Zhou Xiongfei, Lin Jing., : "Deflection Analysis of Clamped Square Sandwich Panels With Layered-gradient Foam Cores Under Blast Loading." *Thin-Walled Structures*, vol. 157, Sept. 2020, p. 107141. 10.1016/j.tws.2020.107141.